Laser Dynamics with Competing Instabilities

F. T. Arecchi,[a] R. Meucci,[b] and W. Gadomski[c]
Istituto Nazionale di Ottica, 50125 Firenze, Italy
(Received 29 December 1986)

Successive transitions from Hopf bifurcation to Shilnikov chaos and eventually to regular spiking are observed in a laser with feedback on increase of a control parameter. Each one of these regimes is due to the dominant attraction of one at a time among three coexisting unstable fixed points. Hence, each situation has a global behavior sufficiently described by attribution of the major part of the return time to a single fixed point.

PACS numbers: 42.50.Tj, 05.45.+b

By operating a CO_2 laser with feedback in a parameter range with three coexisting unstable fixed points, we have found experimental evidence of competition among different instabilities, displaying the successive transition from a Hopf bifurcation to Shilnikov chaos[1-3] and eventually to regular spiking, as a control parameter is monotonically increased. These three regimes are associated respectively with the local behavior around each of the three fixed points. The dynamical behavior consists of closed orbits visiting successively the neighborhoods of the three points. Hence, different regimes are observed when the relative attraction of different ones of the fixed points are dominant. A global model description could be done by composition of successive linearized maps, each one describing the injection into and the departure from a small box around each of the fixed points.[4] However, because of the dominant character of one of the instabilities in each different range of the control parameter, we adopt a simplest interpretation, attributing most of the orbital period around a suitable Poincaré section to the time spent in the vicinity of the dominant fixed point.

A single-mode class-B laser is a good case for the study of chaotic instabilities, since its dynamics is ruled by two coupled degrees of freedom (intensity x and population inversion y).[5] Introduction of a third degree of freedom z by feedback leads to a three-dimensional system displaying oscillatory instabilities and chaos.[6]

The dynamical equations are given by Eq. (1) in Ref. 6, where we also discuss the details of the feedback scheme. There are three control parameters, the bias B, the gain r,[7] and the damping rate β of the feedback loop, all the other parameters being fixed at the values reported in Ref. 6, except the pump, which is here lowered from $A=4.2$ to $A=2.5$ ($A=1$ being the threshold value for laser action).

The experimental information consists of phase-space projections on the x-z plane, obtained by our feeding an x-y oscilloscope with a photodetector signal proportional to the laser intensity and with the feedback signal applied to the modulator. For each phase-space portrait the associated time plot $x(t)$ is recorded on a digital oscilloscope.

In Figs. 1 and 2 we report experimental data for two different gain values, and in each case for three increasing B values. The phenomena reported here are independent of β, for β consistently larger than the popula-

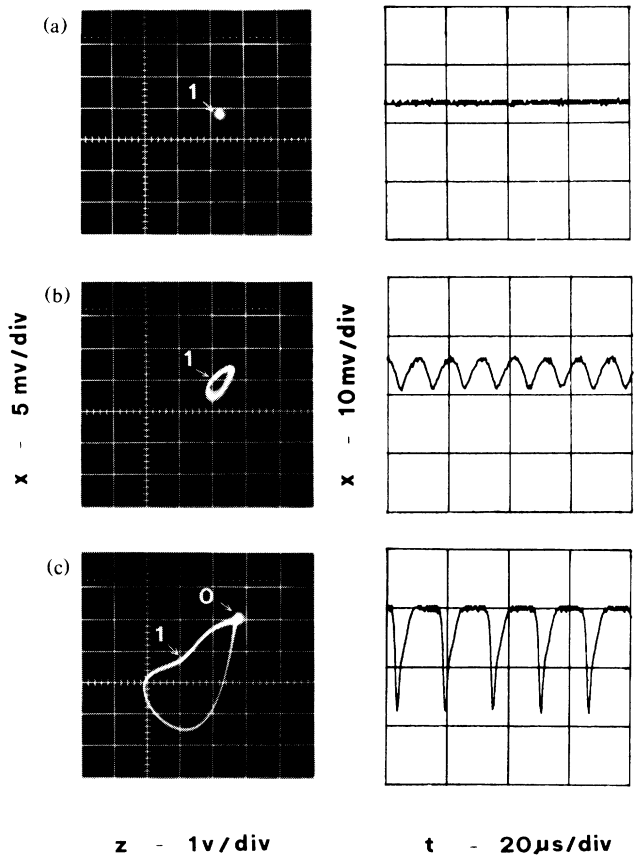

FIG. 1. Phase-space projections z-x [(feedback voltage)-(laser intensity)] and time plots of the intensity $x(t)$ for low feedback gain. Intensity increases downward. Normalization for B as in Ref. 6; (a) $B=0.259$; (b) $B=0.274$; (c) $B=0.385$. Approximate locations in the phase plane of points 1 and 0 are indicated.

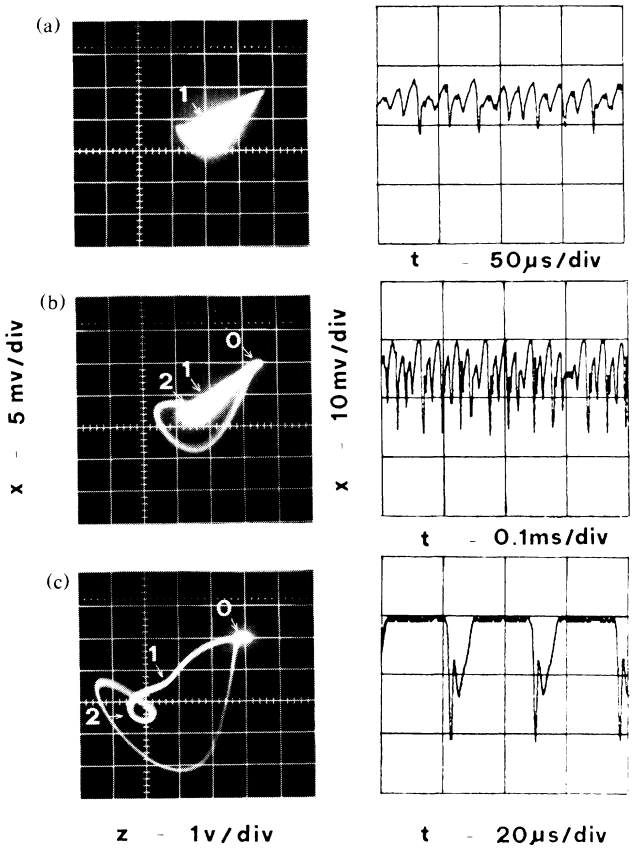

FIG. 2. Phase-space projections z-x [(feedback voltage)-(laser intensity)] and time plots of the intensity $x(t)$ for high feedback gain (between curves c and d of Fig. 2, Ref. 6). (a) $B=0.296$; (b) $B=0.311$; (c) $B=0.411$. Also indicated are the approximate locations of points 0, 1, and 2 in the phase plane.

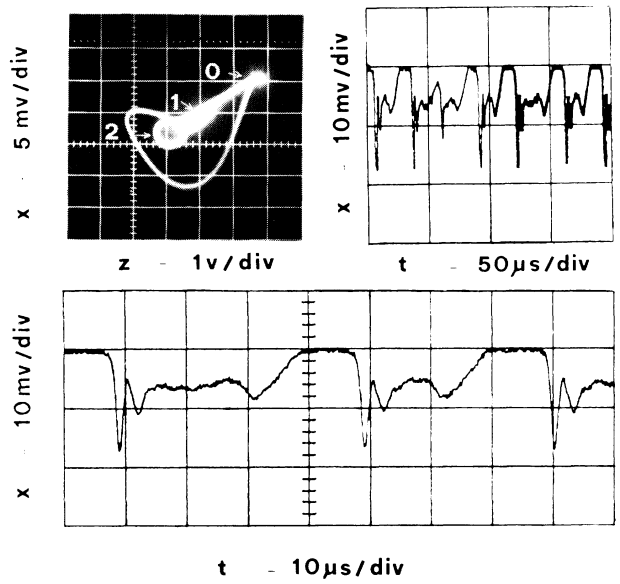

FIG. 3. Phase-space projection and intensity vs time $x(t)$ for the same gain as Fig. 2 and for $B=0.351$. The time-expanded plot $x(t)$ shows clearly the role of the Shilnikov instability in yielding chaotic return times. Approximate locations of points 0, 1, and 2 in the phase plane are indicated.

tion decay rate. We have chosen $\beta/2\pi=400$ kHz; however, a reduction to 100 kHz does not change the observed features. In the phase-space portraits as well as in the time plots, 0, 1, and 2 denote the three fixed points. The fixed points can be localized in a plot of the stationary intensity $\bar{x}$ vs B for different gain values, such as Fig. 2 of Ref. 6. Notice, however, that the change of β and A from that experiment to the present one does not allow an accurate localization of the points in that plot. A linear-stability analysis of the equations of Ref. 6 shows that 0 (zero-intensity solution) is a saddle point with three real eigenvalues, two negative (stable manifold) and one positive (unstable manifold), and 1 turns from a stable point to a Hopf instability (one real negative eigenvalue and two complex conjugate ones with positive real part) for increasing B. For a wide range of B values, 2 has a real positive eigenvalue and two complex conjugate ones with negative real part, and this is the signature of a Shilnikov instability.[4] With this in mind, it is now easy to interpret the experimental facts.

In Fig. 1 (low gain) as B increases, the first fixed point, 1, becomes unstable through a Hopf bifurcation [Fig. 1(b)]. For higher gain, the limit cycle gets unstable and gives rise to chaotic trajectories, as we will see below in discussing Fig. 2(a). As the loop gets wider, it eventually approaches 0 (the zero-intensity solution). This implies a long pause, since the laser is nearly extinguished and must wait a long build-up time before revisiting the region of phase space where the other fixed points are located. This pause has a stabilizing action since the strong contractions associated with the stable manifold of 0 damps the fluctuations built over the previous cycle. Eventually, the return time is dominated by this pause. The loop then corresponds to narrow spikes, slightly perturbed by the attraction of point 1, plus a long lethargy time in the vicinity of point 0 [Fig. 1(c)].

For high gain, two new important features appear. First, the Hopf bifurcation around 1 gives rise to a subharmonic route to a local chaos, as already described in Ref. 6. Figure 2(a) shows the chaotic motion installed at the end of the subharmonic sequence. If we increase B further, the chaotic trajectory widens and eventually it gets close to the fixed point 2 [Fig. 2(b)]. The time spent near 2 fluctuates because the trajectory is sensitively dependent on the initial coordinates of approach, as described in detail in Ref. 1–4 (Shilnikov chaos).

As the phase point goes nearer to 2, the escape time gets longer, so that eventually the time spent around 2 is larger than that around 1 or around 0, thus characterizing the global behavior (Fig. 3). But, once 0 has been

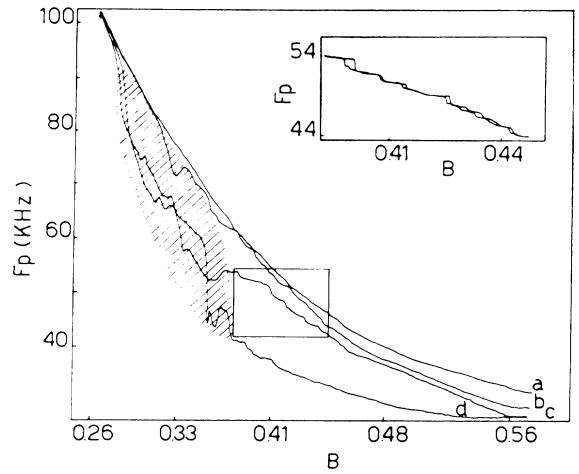

FIG. 4. Plot of the Poincaré frequency f_p vs bias B for four different gain values a to d: increasing gain. Curves a and d refer to the gain values of Fig. 1 and Figs. 2 and 3, respectively. Curve c displays a steplike feature with hysteresis, as clearly shown in the expanded inset of the square region. The shaded region refers to a chaotic f_p; hence the traces reported within that region are just a single scan, while different ones range over the shaded region. Outside the shaded region the curves are fully repeatable.

reached; the interplay between contraction and expansion rates reduces the amount of fluctuations built around the Shilnikov instability, thus regularizing the return time and giving rise to narrow and equally spaced spikes [Fig. 2(c)].

If we now disregard the local features of the phase-space motion and look for a global indicator, the most convenient one is the return time after one whole loop. This is measured experimentally by an average rate meter. Figure 4 shows the behavior of the average Poincaré frequency f_p (reciprocal of the return time) versus the bias B, for several gain values.

For low gain, f_p has a monotonic decrease versus B. Initially, it corresponds to the Hopf frequency around 1, but, as the attraction of 0 prevails, f_p becomes the reciprocal of the occurrence time of the narrow spikes. For high gain, besides the irregular regime where f_p is undefined because of strong chaotic changes (shadowed region) a novel feature is the appearance of vertical steplike jumps, including hysteresis at each jump (see expanded inset in Fig. 4). This is equivalent to forbidden frequency values, just the opposite of what occurs in locking phenomena where there are horizontal steps in frequency.

We have thus seen that the above dynamics with competing instabilities can be divided into three regimes, each corresponding to a dominant fixed point: (i) For low B the motion starts at 1 and for increasing B we have a Hopf bifurcation, followed by a subharmonic route to chaos; (ii) for high B, the motion is a regular periodic spiking with no memory of other features (0 dominant); (iii) at intermediate B (2 dominant), the Shilnikov instability provides chaotic fluctuations in the return time. While region (i) was already described in Ref. 6, a few qualitative remarks are appropriate for the other two regimes.

We can treat regime (ii) in the limit of large β, where the feedback voltage z adjusts instantaneously to the laser intensity. In order to cope with the sharp spikes, it is more convenient to switch notation to a logarithmic representation of the intensity, $s=\ln x$.[8,9] The two remaining equations (1) of Ref. 6 reduce to a single one, second order in s. In the absence of feedback ($z=0$) and for a small ratio between population and photon decay rates (this ratio is 10^{-3} for our CO_2 laser), the equation reduces to that of a lossless Toda oscillator whose period is easily evaluated.[9] By extending the treatment of Ref. 9 to include the feedback[10] we obtained an increasing Poincaré period versus B, in qualitative agreement with the experimental data of Fig. 4.

In regime (iii) we take the opposite limit, namely, that most of the return time is spent within a small distance of fixed point 2. The time $\bar{t}$ spent in the unit box around that point is shown in Ref. 4 to vary as $\bar{t}\simeq\ln(1/z_0)$ where z_0 is the offset at the box entrance along the expanding direction. As the system moves from 1 dominant to 2 dominant, it is reasonable to take $1/z_0$ proportional to the bias B, since for larger B the phase point comes closer to fixed point 2. Hence, the above solution yields a frequency $f_p=1/\bar{t}$ monotonically decreasing with B, in qualitative agreement with the average trend of Fig. 4. However, to explain the steplike details, we must consider two contracting directions, that is, the three-dimensional character of the spiral at the Shilnikov instability. In this case the corresponding return map[4] can be modeled in terms of a number of loops corresponding to the number of jumps in the expanded plot of Fig. 4, thus making it possible to evaluate the complex contraction rate and the real expansion rate of the Shilnikov instability.

A detailed correspondence between the model of Ref. 4 and our physical system is given in a forthcoming paper,[10] together with a global theoretical picture of the phenomena here reported.

We are very grateful to P. H. Coullet for having clarified some aspects of our dynamical system, to S. Ciliberto and J. A. Roversi for useful discussions, to A. Lapucci for help in the measurement, and to N. B. Abraham for revision of the manuscript.

---

[a]Also at Department of Physics, University of Florence, Italy.

[b]On leave from Istituto di Cibernetica del Consiglio Nazionale delle Ricerche, Arco Felice, Napoli, Italy.

[c]Visiting from Department of Chemistry, University of

Warsaw, Poland.

[1]A. Arneodo, P. H. Coullet, and C. Tresser, J. Stat. Phys. **27**, 171 (1982).

[2]L. P. Shilnikov, Dokl. Akad. Nauk SSSR **160**, 558 (1965) [Sov. Math. Dokl. **6**, 163 (1965)].

[3]L. P. Shilnikov, Mat. Sb. (N.S.) **77**, 461 (1968), and **81**, 92 (1970) [Math. USSR-Sb. **6**, 427 (1968), and **10**, 91 (1970)].

[4]A. Arneodo, P. H. Coullet, E. A. Spiegel, and C. Tresser, Physica (Amsterdam) **14D**, 327 (1985).

[5]F. T. Arecchi, in *Instabilities and Chaos in Quantum Optics,* edited by F. T. Arecchi and R. G. Harrison (Springer-Verlag, Berlin, 1987).

[6]F. T. Arecchi, W. Gadomski, and R. Meucci, Phys. Rev. A **34**, 1617 (1986).

[7]For convenience we recall that the voltage z applied to the electro-optic modulator controlling the cavity losses is related to the laser intensity x via a factor r (which in Ref. 6 was called f) accounting for photodetector efficiency and amplifier gain, plus a bias B added to the second input of the feedback amplifier. The transfer from $rx+B$ to z is mediated by a low-pass filter with time constant $1/\beta$.

[8]A. M. Ratner, *Spectral, Spatial and Temporal Properties of Lasers* (Plenum, New York, 1972).

[9]G. L. Oppo and A. Politi, Z. Phys. B **59**, 11 (1985).

[10]F. T. Arecchi, P. H. Coullet, R. Meucci, and J. A. Roversi, to be published.

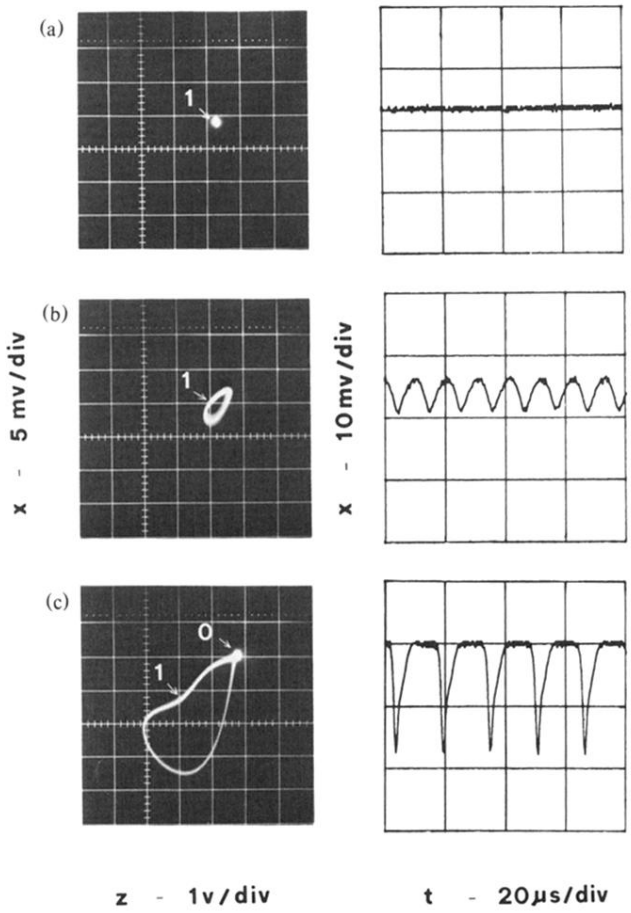

FIG. 1. Phase-space projections z-x [(feedback voltage)-(laser intensity)] and time plots of the intensity $x(t)$ for low feedback gain. Intensity increases downward. Normalization for B as in Ref. 6; (a) $B=0.259$; (b) $B=0.274$; (c) $B=0.385$. Approximate locations in the phase plane of points 1 and 0 are indicated.

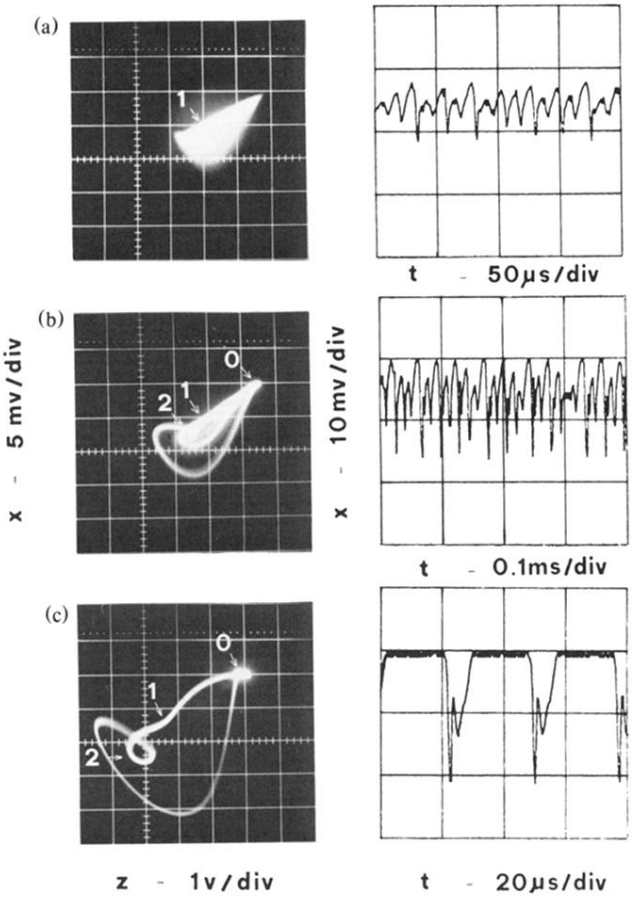

FIG. 2. Phase-space projections z-x [(feedback voltage)-(laser intensity)] and time plots of the intensity $x(t)$ for high feedback gain (between curves c and d of Fig. 2, Ref. 6). (a) $B=0.296$; (b) $B=0.311$; (c) $B=0.411$. Also indicated are the approximate locations of points 0, 1, and 2 in the phase plane.

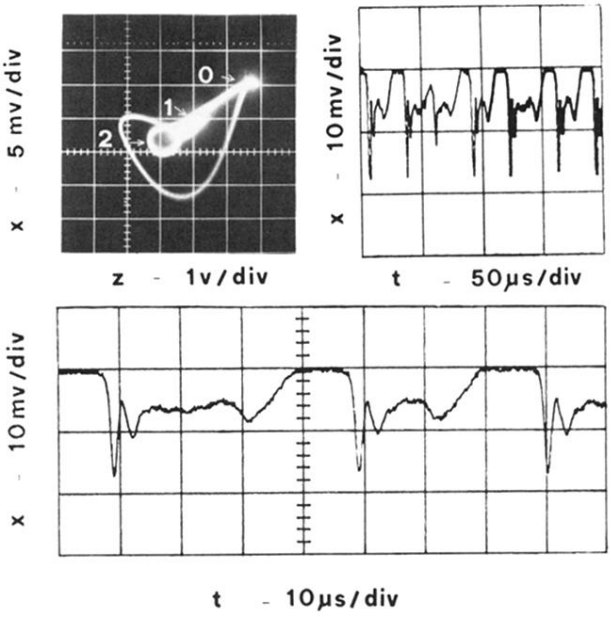

FIG. 3. Phase-space projection and intensity vs time $x(t)$ for the same gain as Fig. 2 and for $B=0.351$. The time-expanded plot $x(t)$ shows clearly the role of the Shilnikov instability in yielding chaotic return times. Approximate locations of points 0, 1, and 2 in the phase plane are indicated.